ORIGINAL PAPER

Room temperature quantum key distribution characteristics of low-noise InGaAs/InP single-photon avalanche diode

Soo-Hyun Baek[1,2] · Seung-Chul Yang[1] · Chan-Yong Park[1] · Chul-Woo Park[3] · Seok-Beom Cho[3] · Sang-Wan Ryu[2]

Abstract

InGaAs/InP single-photon avalanche diode (SPAD) with small active diameter and backside microlens was fabricated and its dark count and after-pulse noises were characterized. In addition, by optimizing multiplication layer and reducing the active diameter, high photon detection efficiency (PDE) was achieved as well as suppressed dark count probability (DCP) and after-pulse probability (APP) near room temperature. The gated Geiger-mode characteristics of SPAD were investigated with the gate amplitude of 6.6 V and repetition frequency of 10 MHz. Superior single-photon detection characteristics as PDE of 20.9%, DCP of 1.02×10^{-5} and APP of 0.8% were observed at the operation temperature of $+20\,°C$. It is a promising result that allows compact and low-cost detector module for quantum key distribution system with simple cooling apparatus.

Keywords Single-photon avalanche diode · Quantum key distribution · Dark count · After-pulse

1 Introduction

The InGaAs/InP avalanche photodiode (APD) has been widely used for optical communication because it showed excellent absorption property at 1550 nm and sufficiently low dark current yielding highly reliable properties. Recently, its application has been extended to single-photon avalanche diode (SPAD) for the application of quantum key distribution (QKD) [1, 2], optical time domain reflectometry and LiDAR receiver [3, 4].

Key issues in applying SPAD to the QKD system application are how to obtain high photon detection efficiency (PDE), low dark count rate or dark count probability (DCP) per gate, and low after-pulse probability (APP). PDE and DCP are very important in QKD system for realizing long distance transmission without repeater. However, DCP and PDE are closely related, i.e., if one increases PDE, then DCP also increases. This correlation is based on high electric field that is required for PDE whereas it increases dark current

multiplication. To reduce DCP without degrading PDE, the volume of InGaAs absorption layer should be minimized because dark current is generated mainly in the InGaAs absorption layer due to its small bandgap. Another way to increase PDE without increasing DCP is to employ a back-entry structure with mirror coating for recycling reflected photons.

Precise control of electric field in the SPAD is another essential factor to control photon detection parameters. Electric field in InP multiplication layer should be sufficiently high to have avalanche multiplication but should be suppressed not to generate dark current from tunneling. The electric field in InGaAs absorption layer also should be controlled very carefully to minimize dark current [5, 6] while allowing fast electron/hole transport into multiplication layer for high speed operation. Thus, it is important to design accurately the multiplication layer width and charge density of field control layer [6] to achieve good performance of SPAD.

The APP affects the operation speed of QKD system. Once an avalanche event takes place, large current will flow through diode. Carriers are captured at defects and emitted with long decay time. If the emitted carrier enters into multiplication region at the next or subsequent gating time, then unwanted noise signals is generated, which is the origin of after-pulse. To reduce APP with conventional gating technique, one should operate SPAD with sufficiently wide

✉ Sang-Wan Ryu
  sangwan@chonnam.ac.kr

1 Wooriro Co., Ltd, Gwangju 62453, South Korea

2 Department of Physics, Chonnam National University, Gwangju 61186, South Korea

3 ID Quantique, Gyeonggi 13595, South Korea

interval between gates, but it decreases the operation speed in QKD system. The several techniques to reduce the afterpulse, such as sine-wave gating technique [7], self-differencing technique [8], and dual-anode SPAD technique [9], have been introduced and successfully demonstrated at gate frequency around several GHz.

The essential parameters of QKD should be compromised carefully for quantum communication. However, the performance of SPAD is still limited for efficient and reliable system. In this paper, we report the fabrication and characterization of an InGaAs/InP based SPAD with very low DCP and APP even at room temperature. The SPAD with small active area was designed to obtain low DCP and a microlens was formed on the bottom side of InP substrate to increase photon-coupling efficiency.

2 Experimental details

2.1 Design and fabrication of SPAD

Since the critical requirements for SPAD are low dark current, high gain, and the suppression of edge breakdown, the design of epitaxial layers as well as formation of p–n junction by Zn diffusion should be very accurately performed. In this regard, Hi–Lo structure is the best for this purpose and the floating guard ring-type APD is the most suitable to suppress edge breakdown of Hi–Lo APD [10, 11]. Double Zn-diffusion was adopted in this study for separate control of electric fields in absorption and multiplication layers and formation of guard ring outside the periphery of active region [12].

To fabricate SPAD, the epitaxial layers were grown on the n^+-InP substrate to have a 1.5-µm-thick InGaAs absorption layer, 0.15-µm-thick multiple InGaAsP grading layers, a 0.2-µm-thick n-InP field control layer, a 3.0-µm-thick undoped InP window layer, and 0.1-µm-thick an n-InGaAs contact layer. To reduce contact resistance, InGaAs contact layer was initially moderately doped with n-type by 5×10^{17} cm^{-3}. A p–n junction was formed using double Zn-diffusion technique. After diffusion, InP window layer was partially converted into p-InP. The rest of InP remained undoped acts as a multiplication layer. In the active region, n-type InGaAs is converted into p-type during Zn-diffusion. Both of n-type and p-type contacts have been formed simultaneously on n-InGaAs and p$^+$-InGaAs, respectively. Metal electrodes for both cathode and anode were deposited using Ti/Pt/Au at the same time. SiNx passivation layer was deposited using plasma enhanced chemical vapor deposition, and SiNx was etched at metal electrode for electrical contact. During the process, the active diameter of SPAD was varied. The SPADs of 16 µm and 25 µm diameters were fabricated and characterized for their single-photon detection properties.

Then backside processing for microlens follows. After lapping and polishing the processed wafer to have thickness of 150 ± 15 µm, Cr/Au metal pattern is fabricated to be used as an etch mask. The alignment of Cr/Au pattern with the SPAD active region was achieved by backside photolithography technique. An InP microlens with a diameter of 100 µm was formed on backside of InP substrate by inductively coupled plasma reactive ion etching. The radius of curvature and height were about 100 µm and 12 µm, respectively. Finally, anti-reflection film was deposited on lens surface with minimum reflectivity at 1550 nm wavelength. Figure 1 shows the cross-sectional diagram of fabricated SPAD chip. The backside illumination design with both top electrodes is advantageous for flip-chip packaging and reliable optical coupling between the chip and an optical fiber. In addition, it enables the reduction of active dimension without the loss of optical efficiency that results in reduced chip capacitance.

The SPAD chip-on-carrier (CoC) was assembled by flip-chip bonding technique. Front side of SPAD chip faced down to make contact with 2.5- to 3.0-µm-thick Au/Sn solder bump formed on a specially designed quartz carrier. Then, the CoC was mounted on TO-8 header with 3-stage thermo-electric cooler (TEC). TO-8 header consists of 6 pins for electrical connection to the TEC, thermistor and SPAD CoC, respectively. The photograph of SPAD CoC is shown in Fig. 2. Finally, precise optical alignment was performed using three-axis stages for laser welding to construct an optical fiber pigtail.

2.2 Characterization of SPAD

Figure 3 shows linear-mode characteristics to investigate photo and dark currents of the fabricated SPAD. Very low dark current less than 200 pA was obtained. As shown in Fig. 3, Punch-through voltage (V_p) is the voltage at which the depletion of the InGaAs absorption layer begins, and it can be seen that V_p of the device fabricated in this study is located at 40–50 V. Near the V_p, the photocurrent increases abruptly because InGaAs absorption layer begins the depletion and photo-generated holes enter into multiplication region by overcoming potential barrier originating from the valence band discontinuity between InP and InGaAs. Breakdown voltage (V_B), defined by the voltage that dark current exceeds 100 µA, was 70 V. In general, V_B increases as the temperature increases. Temperature coefficient (γ), defined by $\gamma = \Delta V_B / \Delta T$, is measured 0.1 V/°C. The chip capacitance, not shown here, was 142 fF, which is small enough for high-speed operation. Furthermore, the small capacitance will reduce the amplitude of capacitive response, which results in relatively low APP.

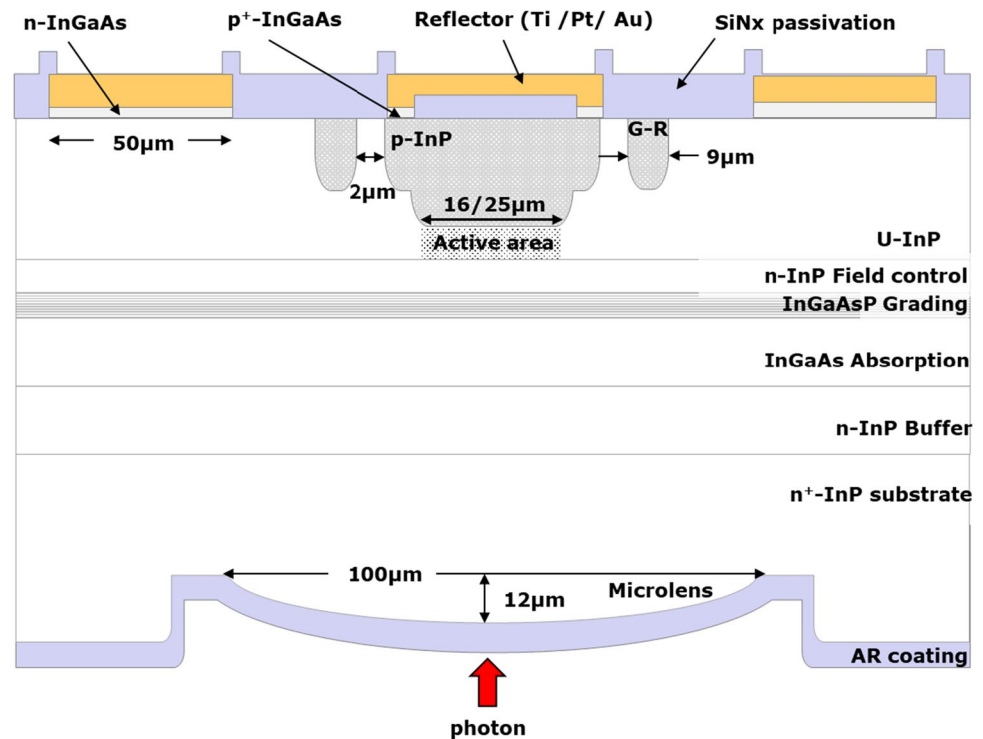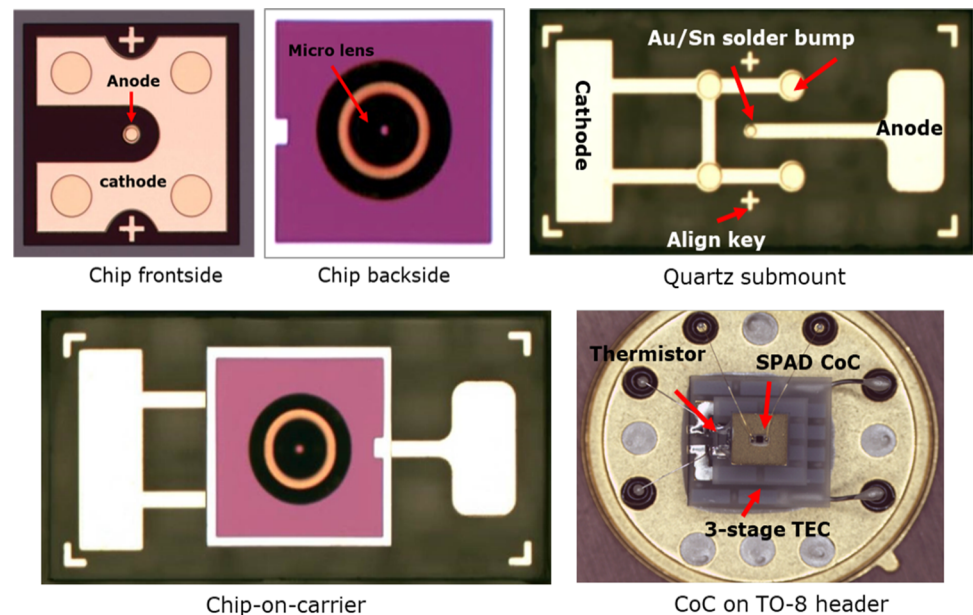**Fig. 1** Cross-sectional diagram
of designed SPAD

Fig. 2 Photograph of the fab-
ricated SPAD chip-on-carrier
(CoC) and TO-8 header

2.3 Single-photon detection measurements

For single-photon detection, the avalanche photodiode must
be operated in a Geiger-mode, providing the gain of SPAD
more than 10^4. However, when the avalanche photodiode is
operated in Geiger mode, an incident optical signal causes
successive amplification with long decay time. In this situa-
tion, it is difficult to distinguish an incident signal from sub-
sequent incidence. Therefore, the SPAD must be operated

in a fast quenching mode of the photoresponse. In the gated
mode, a voltage higher than the V_B is applied only when an
optical signal is input to the avalanche photodiode, and at
other times, the voltage is slightly lower than V_B. The section
in which the voltage is periodically raised for a short period
of time is called a gate, and the gate frequency becomes the
operating speed.

In general, the gate frequency can be operated from
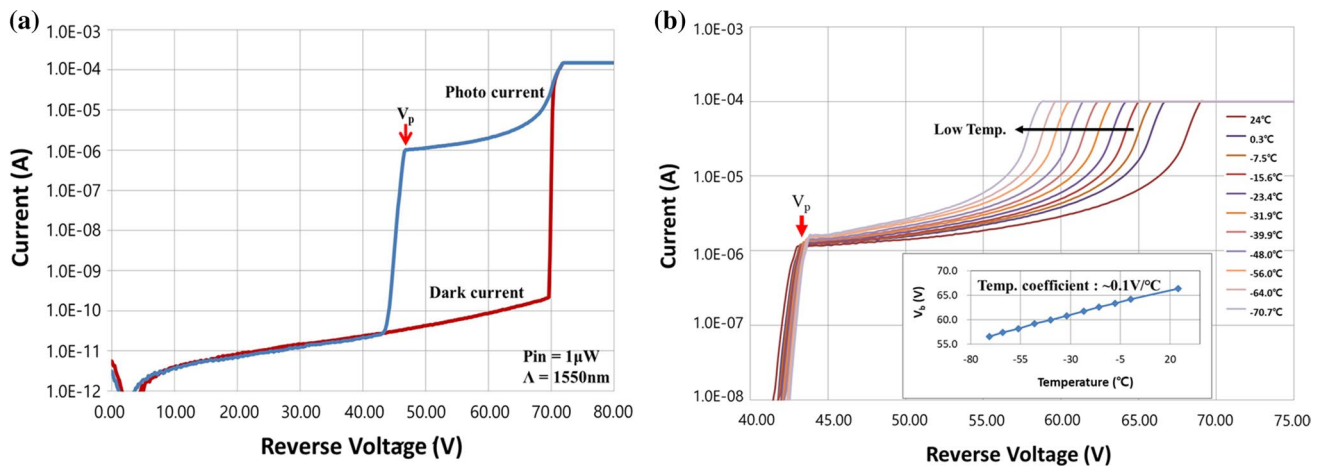several MHz to GHz. Gated Geiger-mode performance

Fig. 3 **a** Typical photocurrent and dark current characteristics of SPAD. **b** Variation of avalanche gain curve with temperature. The incident laser wavelength and power were 1550 nm and 1 μW, respectively. The inset shows the variation of breakdown voltage with temperature

was measured using conventional gating technique shown in Fig. 4a. The gate bias (V_G) was set at the fixed value of 6.6 V with 2 ns gate width and repetition rate of 10 MHz, while DC bias was adjusted close to V_B to obtain the desired PDE. The gated Geiger-mode QKD experimental setup was configured as shown in Fig. 4b. A DFB-LD with 1550-nm wavelength and 190 ps pulse width was used for photon pulse generation. Optical pulse from DFB-LD is controlled by variable optical attenuator (VOA) to have averaged photon number of 0.1 per pulse. To evaluate SPAD performance at various temperatures, the temperature of the chip was adjusted from − 40 °C to + 20 °C using the built-in TEC. Output from SPAD was fed into a discriminator to calculate PDE, DCP, and APP.

3 Results and discussion

We first compared the capacitive response of output signals in dark from the two fabricated SPADs with 16-μm and 25-μm active area. This response constructs the baseline for the discrimination of photon detection. Figure 5 displays the capacitive response signal of a SPAD operated in gated Geiger-mode the scheme of which was illustrated in Fig. 4a. Since such a capacitive response signal limits the minimum threshold for the discrimination, it is necessary to minimize its peak-to-peak amplitude. From the figure, the peak-to-peak amplitude of the SPAD was measured 52 mV and 89 mV for 16-μm and 25-μm active area devices, respectively. Capacitive response amplitude was proportional to the light-receiving area which was attributed to the high
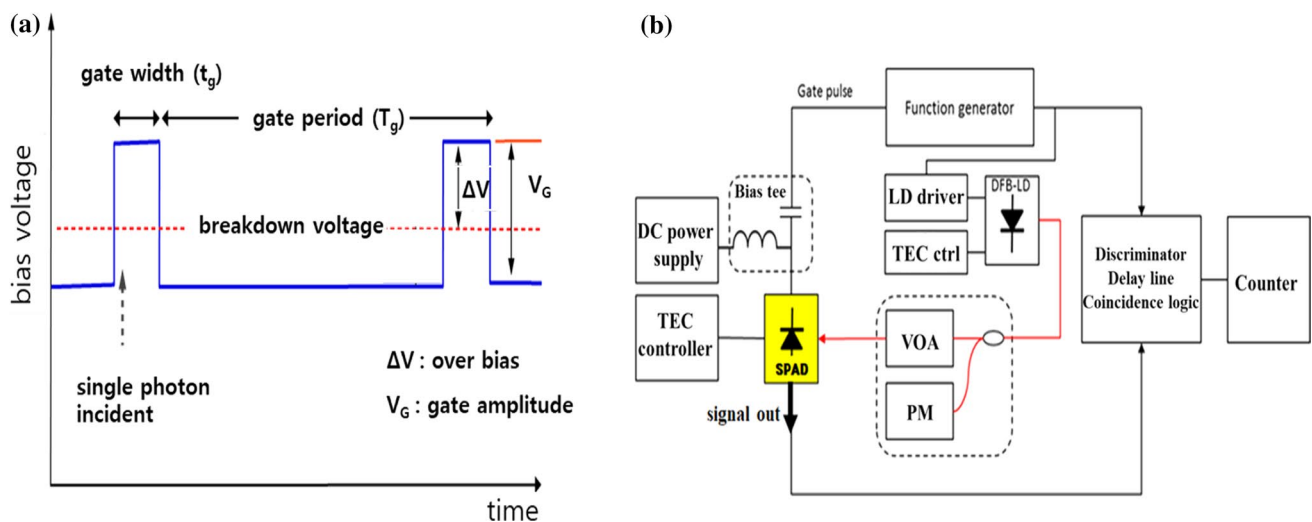

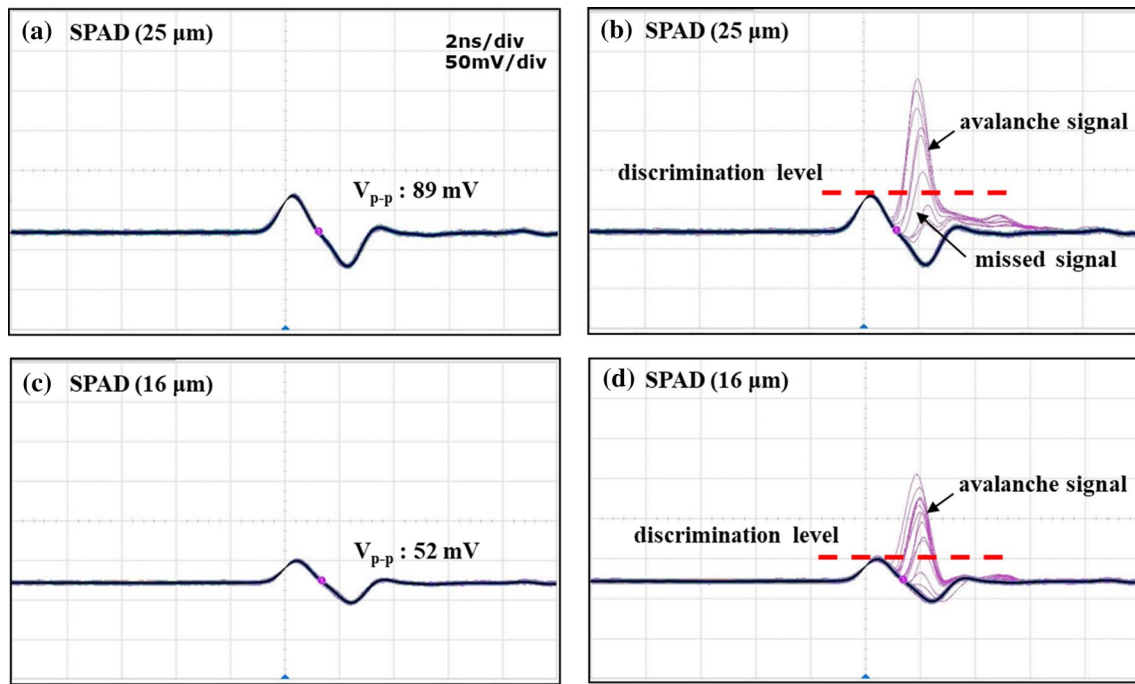**Fig. 4** Circuit diagram of the conventional gated Geiger-mode experimental setup for SPAD performance

Fig. 5 **a**, **c** Measured capacitive response and **b**, **d** avalanche output signal of SPADs of different active diameters. The horizontal and vertical divisions represent 2 ns and 50 mV, respectively

capacitance of large area SPAD. Therefore, the SPAD of 16-μm active area can discriminate weak avalanche signal more effectively than that of 25-μm active area (see Fig. 5b, d). Owing to the low discrimination level, relatively low DC bias could be used for the same photon detection efficiency, which in turn reduced the noise characteristics such as DCP and APP.

The optimal performance of SPAD was investigated for various gate biases. The important QKD parameters such as DCP and APP were compared while varying the gate bias from 5.0 to 6.6 V. At the same time, DC bias was controlled to meet the designated PDE value. DCP was calculated as R_{dark}/f_g, where R_{dark} is the dark count rate measured without photon injection into the SPAD, f_g is the gating frequency. PDE and APP is calculated as [13, 14]

$$\text{PDE} = (1/\mu) \times \ln\left[(1 - \text{DCP})/(1 - R_{det}/f_p)\right], \quad (1)$$

$$\text{APP} = \left[R_{total} - R_{det} - \left(1 - f_p/f_g\right)R_{dark}\right]/R_{det}, \quad (2)$$

where μ is the average photon number, R_{total} is the rate of the detection events at all gates, R_{det} is the rate of the detection events occurring at the gates receiving optical pulse only and f_p is the frequency of laser triggered to the gate pulse.

Figure 6a, b shows typical DCP and APP properties as a function of PDE for the SPAD of 16-μm active region. There was no significant difference in DCP, however, the best APP was obtained at 6.6 V gate bias. The meaningful

difference of APP was observed only at high PDE of 30% and it decreased from 7.31 to 4.89% as the gate bias was increased from 5.0 to 6.6 V. This sharp increase of APP with PDE is believed to originate from large DC bias required for the high PDE. Large V_G of 6.6 V is adopted to keep the DC bias low while the applied bias in a gating period (DC bias + V_G) is large enough to enhance the PDE. The gate bias higher than 6.6 V could not be tested due to the limitation of the gate amplifier. Due to the significant influence of DC bias on QKD parameters, their dependence on DC bias was separately measured and displayed in Fig. 6c, d.

In general, SPAD is cooled down to the temperature around − 40 °C by 3-stage TEC for low dark noise operation. It increases the power consumption, footprint, and cost of single-photon detection module. By these reasons, room temperature operation of SPAD is one of key issues for current QKD system. It should be noted that a single-stage TEC is mandatory even with the room temperature operating SPAD due to the abrupt change of breakdown voltage by temperature. However, it releases significantly the burden of using 3-stage TEC and related footprint and power consumption issues. To examine the temperature characteristics, SPAD was cooled down to − 40 °C by TEC control and the temperature was increased to + 10 °C and + 20 °C. Figure 7 shows measured DCP and APP values for five selected devices at three temperatures. DCP as well as PDE is a limiting parameter for the distance of quantum communication. The DCP shown in Fig. 7a, c
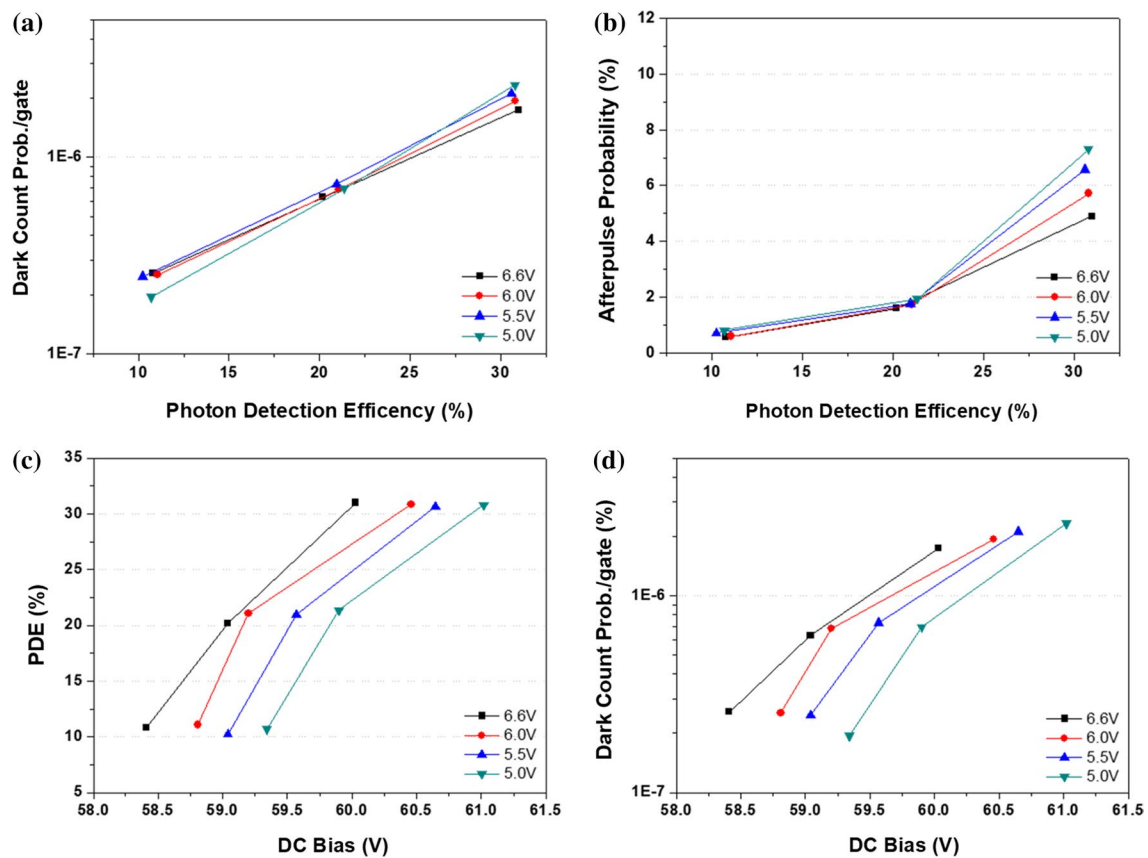
Fig. 6 **a**, **b** DCP, APP vs. PDE and **c**, **d** PDE, DCP vs. DC bias for various gate bias at −40℃

exhibited abrupt increase with the temperature for both devices; DCP at +20 °C was higher than that at −40 °C by roughly order of two. Besides, DCP increases with PDE, too. However, it clearly shows the dependence on the active size. At the same PDE and temperature, the SPAD of 16-μm active area displays lower DCP all the time, which originated from small capacitive response amplitude. It is known that DCP should be smaller than 2×10^{-5} per gate for conventional QKD system. The SPAD of 16-μm active area satisfies this criterion at +20 °C for PDE less than 25%. This is a meaningful result for its application for room temperature quantum communication.

Furthermore, APP is a parameter that limits the QKD data rate. The APP shown in Fig. 7b, d exhibited gradual decrease with the temperature while it increased significantly with PDE. The lower APP at the higher temperature is attributed to enhanced carrier emission rate from defect center in the multiplication layer. APP should be less than 3% for the QKD system, so it limits the maximum PDE. The SPAD of 25-μm active area shows higher APP except low PDE regime. However, SPAD of 16 μm satisfies the requirement for all PDE values at +10 °C and +20 °C. It even shows very low APP less than 1% at +20 °C when PDE is smaller than 20%.

Even though high PDE is favorable for high speed key distribution, in our experiments, we did not include the condition for high PDE over 30% to prevent gradual increase of DCP and APP. The low DCP and APP at room temperature makes it possible to fabricate SPAD with a single-stage TEC to have a smaller size package such as TO-46 or TO-56 instead of 3-stage TEC resulting in mass-production for low-cost solution. Therefore, the PDE and other noise characteristics should be carefully compromised. Consequently, at 20% PDE, single-photon detection was demonstrated showing DCP of 1.02×10^{-5} per gate and APP of 0.8% at temperature of +20 °C. It satisfied the general requirements as DCP $< 2 \times 10^{-5}$ per gate and APP $< 3\%$ for QKD systems [15]. It showed that the SPAD fabricated in this study can be operated at room temperature instead of commonly used temperature of −40 °C. Therefore, it is expected to have advantages such as simplification of heat dissipation system compared to cryogenic operation and higher operating temperature of commercialized QKD systems.
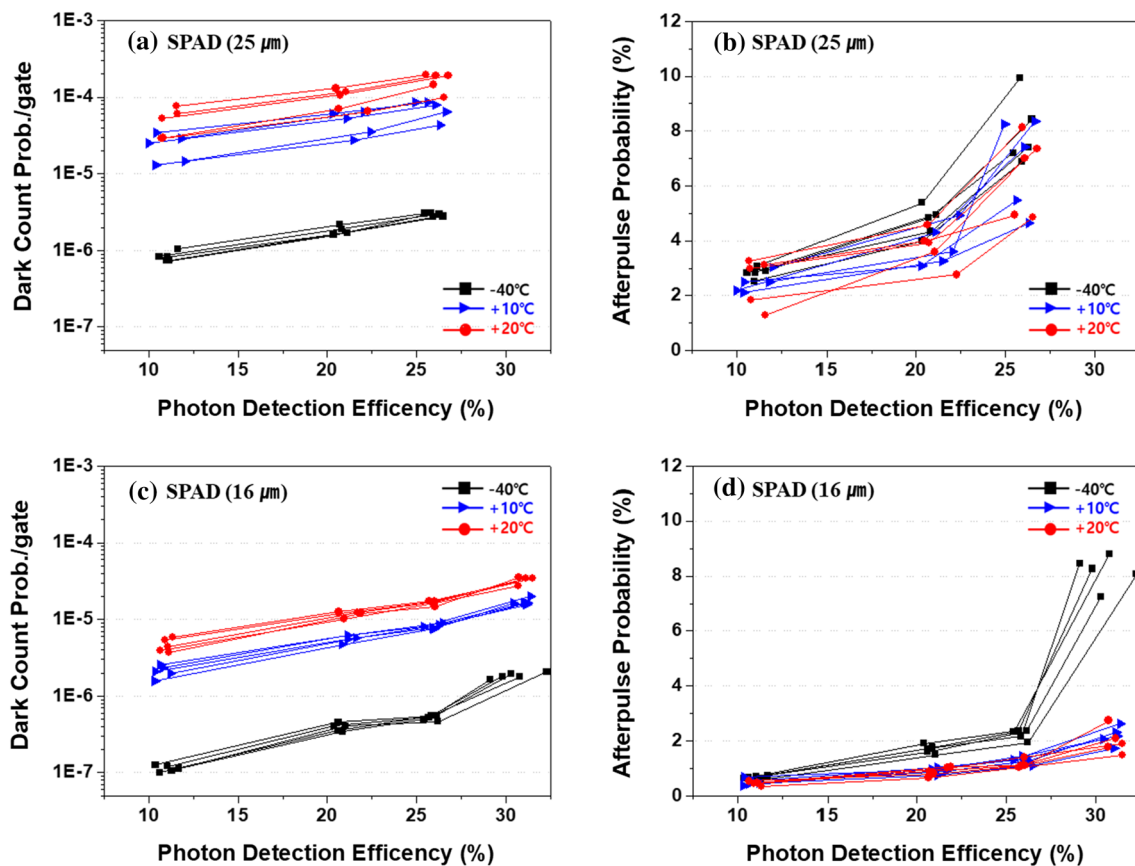
Fig. 7 Measured **a**, **c** DCP and **b**, **d** APP vs. PDE. **a**, **b** was obtained from 25-μm active area SPAD and **c**, **d** was from 16-μm active area SPAD

4 Conclusion

A SPAD with small active volume was integrated with backside microlens for high-performance QKD operation. Enhanced PDE together with reduced DCP and APP was obtained by optimal multiplication layer design and well-controlled Zn-diffusion process. Gated Geiger-mode operation was adopted and its control parameters such DC bias and gate voltage were investigated for balancing PDE and noise characteristics at various temperatures.

DCP was reduced by almost an order of magnitude when the active diameter decreased from 25 to 16 μm at the same PDE, which was attributed to reduction of capacitance and volume of InGaAs absorption layer. The reduction of the active diameter is due to the ability of microlens to focus photons well into the small active area.

In this regard, acceptable DCP of 1.02×10^{-5} per gate was achieved at 20% PDE near room temperature. At the same condition, APP as small as 0.8% was achieved. These results clearly confirm that QKD operation of long distance and high transmission capacity can be demonstrated with the proposed design.

References

1. C. Bennett, G. Brassard, Theoret. Comput. Sci. **560**, 7–11 (2014)
2. E. Ak, Phys. Rev Lett. **67**(6), 661–663 (1991)
3. A.L. Lacaita, P.A. Francese, S.D. Cova, G. Riparmonti, Opt. Lett. **18**(13), 1110–1112 (1993)
4. C. Yu et al., Opt. Express **25**(13), 14611–14620 (2017)
5. X. Meng et al., Opt. Express **22**(19), 22608–22615 (2014)
6. Y. Zhao et al., Opt. Express **19**(9), 8546–8556 (2011)
7. Z.L. Yuan, B.E. Kardynal, A.W. Sharpe, A.J. Shields, Appl. Phys. Lett. **91**(4), 041114 (2007)
8. L.C. Comandar et al., J. Appl. Phys. **117**(8), 083109 (2015)
9. C.W. Park et al., Opt. Express **27**(13), 18201–18209 (2019)
10. D.E. Ackley et al., IEEE Photonics Technol. Lett. **2**(8), 571–573 (1990)
11. C.Y. Park et al., Inst. Phys. Conf. Ser. No **145**, 1125–1128 (1995)
12. K.S. Hyun, C.Y. Park, J. Appl. Phys. **81**(2), 974–984 (1997)

13. J. Zhang, R. Thew, C. Barreiro, H. Zbinden, Appl. Phys. Lett. **95**(9), 091103 (2009)
14. S.B. Cho, S.K. Kang, Opt. Express **19**(19), 18510–18515 (2011)
15. N. Gisin, G. Ribordy, W. Tittel, H. Zbinden, Rev. Mod. Phys. **74**(1), 145–195 (2002)

Publisher's Note Springer Nature remains neutral with regard to jurisdictional claims in published maps and institutional affiliations.